sustainability

MDPI

Article

Rheological and Fatigue Characteristics of Asphalt Mastics and Mixtures Containing Municipal Solid Waste Incineration (MSWI) Residues

Ling Xu [1], Yinfei Du [2], Giuseppe Loprencipe [3,*] and Laura Moretti [3]

[1] Key Laboratory of Road and Traffic Engineering of Ministry of Education, Tongji University, No. 4800 Cao'an Road, Jiading District, Shanghai 201804, China; lxu@tongji.edu.cn
[2] School of Civil Engineering, Central South University, Changsha 410075, China; yfdu_csu@csu.edu.cn
[3] Department of Civil, Constructional and Environmental Engineering, Sapienza University of Rome, via Eudossiana 18, 00184 Rome, Italy; laura.moretti@uniroma1.it
* Correspondence: giuseppe.loprencipe@uniroma1.it; Tel.: +39-0644585112

Abstract: The large-scale implementation of municipal solid waste incineration (MSWI) has put great pressure on waste management and environmental protection. Road construction engineering has also been confronted with the challenges of the heavy consumption of non-renewable mineral resources. Therefore, we evaluated the feasibility of recycling and reusing MSWI residue as an alternative to limestone filler (LF) in transport infrastructure. We investigated the rheological characteristics and fatigue performance of asphalt mastics and mixtures containing MSWI residue. Firstly, a particle size analyzer and environmental scanning electron microscope were adopted to characterize the particle distribution and surface micromorphology of the investigated fillers, respectively. Then, tests for determining the steady shear viscosity and multiple-stress creep recovery were conducted to evaluate the high-temperature rheology of five asphalt mastics. Meanwhile, we used Burgers models with fitting parameters to describe the classic creep recovery measurements and viscoelastic responses. The wheel-tracking test revealed the rutting resistance, and the linear amplitude sweep (LAS) and time sweep tests were combined to investigate the fatigue performances of the five asphalt mastics. A dynamic creep test identified the fatigue life of the asphalt mixtures according to the flow number index. Finally, statistical analysis was conducted to identify the correlations between the rheological and fatigue properties of the mastics and mixtures (R^2 over 0.87 and 0.78, respectively). Since the fatigue life predictions for the asphalt mastic decreased by over 42.9% according to the MSWI residue/LF volume ratio, the results of the correlations could improve pavement designs. The substitution of the mineral filler in asphalt mixtures with MSWI residue could be a sustainable strategy for the road construction sector.

Keywords: municipal solid waste incineration; MSWI; asphalt pavement; rheology characteristics; fatigue performances

check for updates

Citation: Xu, L.; Du, Y.; Loprencipe, G.; Moretti, L. Rheological and Fatigue Characteristics of Asphalt Mastics and Mixtures Containing Municipal Solid Waste Incineration (MSWI) Residues. *Sustainability* **2023**, *15*, 8356. https://doi.org/10.3390/su15108356

Academic Editor: Filomena Ar dolino

Received: 15 March 2023
Revised: 13 May 2023
Accepted: 18 May 2023
Published: 21 May 2023

Copyright: © 2023 by the authors. Licensee MDPI, Basel, Switzerland. This article is an open access article distributed under the terms and conditions of the Creative Commons Attribution (CC BY) license (https://creativecommons.org/licenses/by/4.0/).

1. Introduction

Municipal solid waste (MSW) disposal approaches involve various treatments at different development levels (e.g., thermal processes [1,2], anaerobic co-digestion [2], composting [3], and landfill bioreactors [4,5]). Among these, incineration is the most frequently adopted because of its matured technology, high volume reduction, and small land footprint [6,7]. Incineration can achieve approximately 80% energy recovery for heating or 20–30% energy recovery for electricity [8]. Meanwhile, about 30% of the mass can be used to generate inert residues, also called municipal solid waste incineration (MSWI) residues [9,10].

MSWI residues result from coal-burning processes [11,12] or energy plants [13], and their disposal requires a solution. Usually, MSWI residues are stockpiled and occupy large

areas of fields [14]. However, disposal areas are gradually becoming less able to accommodate redundant MSWI residues. Therefore, researchers and workers have proposed the use of increasing amounts of MSWI residues in construction engineering. For example, the application of MSWI residues to partially replace light aggregates or sand has been promoted in the European construction industry, including in France (70%), Germany (80%), Denmark (90%), and the Netherlands (over 90%) [2]. Indeed, research on MSWI focusing on applicability improvement, performance enhancement, and pollution minimization has increased [8,9].

Researchers have identified beneficial applications of MSWI products, including mine remediation, building construction, landfill cover, Portland cement concrete, and road materials. Their use in the construction field has attracted the most interest [15]. Researchers have investigated the wide-ranging applications of MSWI residues and have confirmed the potential for environmental pollution prevention and the technical opportunities offered by this material [3,16]. Regarding the road construction sector, MSWI residues were employed with alkaline activators to stimulate and accelerate pozzolanic reactions in reclaimed asphalt pavement (RAP) stabilized with MSWI products [17]. A faster geo-polymerization reaction was found to fill the voids of the RAP–MSWI residue mixture with calcium silicate hydrate (C-S-H). Similar observations were reported for MSWI residue-stabilized lateritic soil with a low Na_2SiO_3/NaOH content, which required a longer curing process to produce significant amounts of C-S-H gel [18]. The toxicity characteristic leaching procedure (TCLP) showed that mixtures composed of a reclaimed asphalt pavement and MSWI residue blend did not present significant leaching hazards to groundwater and soil, indicating their safety as a base layer for sustainable roads [19]. However, the pozzolanic reaction ignited by nano silica and MSWI residue improved the early strength development of high-volume MSWI residue roller-compacted concrete with crumb rubber [20], and the compressive strength loss from the crumb rubber was also mitigated.

Nevertheless, the most appropriate means of implementing MSWI residues in road construction is through incorporation with inorganic materials because the application of MSWI residues in asphalt materials is relatively limited [21], despite the increasing demand for asphalt pavements [22,23]. Most research on asphalt pavement containing MSWI residues has focused on simple mechanical performance evaluations, overlooking the knowledge gap regarding the rheological and fatigue characteristics of this material. The reasonable use of MSWI residues in transport infrastructure could mitigate the shortage of natural aggregates [24] and the persistent and serious environmental issues faced by cities [25].

2. Goals and Objectives

This study aimed to investigate the possibility of using MSWI residues to replace natural mineral filler in asphalt materials. Therefore, systematic evaluations of the high-temperature rheological and fatigue characteristics of asphalt materials containing MSWI residues were necessary. The main novelty of this study was the evaluation and identification of relationships between the rheological and fatigue properties of mastics and mixtures from the perspective of the viscoelastic characteristics, which could improve pavement design using MSWI residues. The low absorbability of MSWI residues in asphalt materials was one of the main limitations of this study. Surface treatments and coupling modifiers are suggested for future research to enhance the microstructural properties of MSWI residues and their interaction with asphalt. The study contributions are as follows:

(1) Firstly, particle size and environmental scanning electron microscope (ESEM) tests were used to compare the microscopic characteristics of limestone filler (LF) and MSWI residue;
(2) Several dynamic shear rheometer (DSR) tests, including the zero-shear viscosity (ZSV) and multiple-stress creep recovery (MSCR) tests, were conducted to measure the high-temperature properties of the mastics. Meanwhile, a wheel-tracking test was performed to assess the mixtures;

(3) Linear amplitude sweep (LAS) and time sweep tests were combined to evaluate the fatigue properties of the mastics, while the fatigue resistance of the mixtures was determined through a dynamic creep test;
(4) Finally, the correlations between the high-temperature and fatigue properties of both the mastics and the mixtures were analyzed.

3. Materials and Methods

3.1. Materials

3.1.1. Bitumen

We used PG 64-22 bitumen, whose properties are listed in Table 1, according to the Chinese standard JTG E20-2011 [26].

Table 1. Properties of Paving Asphalt PG 64-22 bitumen.

Property	Unit	Value	Technical Requirement
Penetration, 25 °C, 100 g/5 s	0.1 mm	66	60–80
Softening point	°C	48.5	≥45
Ductility, 5 °C	cm	>100	≥100
Specific gravity	g/cm^3	1.090	-

3.1.2. Asphalt Mastic

Two kinds of mineral powder were used as fillers for asphalt mastic. The limestone filler (LF) was obtained by limestone grinding, and the MSWI residue comprised the bottom ash from an incineration plant. Both fillers were passed through a 0.075 mm sieve, and Table 2 lists their basic properties. In the asphalt mastic, MSWI residues were incorporated by replacing LF at an equal volume.

Table 2. Physical properties of LF and MSWI residue.

Filler	Acronym	Density (g/cm^3)	Appearance
Limestone filler	LF	2.77	White powder
Municipal solid waste incineration residue	MSWI	0.72	Gray spherical particles

Table 3 presents the recipes of the five investigated asphalt mastics with various LF-to-MSWI residue ratios. Different contents of LF and MSWI residue were added to bitumen at 160 °C. A high-speed shearing instrument mixed all the components at a 1500 r/min stirring speed for 30 min until a homogenous dispersion was obtained.

Table 3. Recipes of asphalt mastics (% by weight).

Mastic	LF	MSWI	Asphalt
Control mastic	120	0	100
Mastic #1	90	8.3	100
Mastic #2	60	16.6	100
Mastic #3	30	24.9	100
Mastic #4	0	33.2	100

3.1.3. Asphalt Mixture

The stone mastic asphalt mixture (SMA-13) with a maximum nominal particle size of 13.2 mm was included as the control, because it is commonly used for flexible pavements. The red curve in Figure 1 shows the aggregate gradation. Similarly, the mass ratios of the LF and MSWI residues in the asphalt mixtures were consistent with asphalt mastics (Table 3).

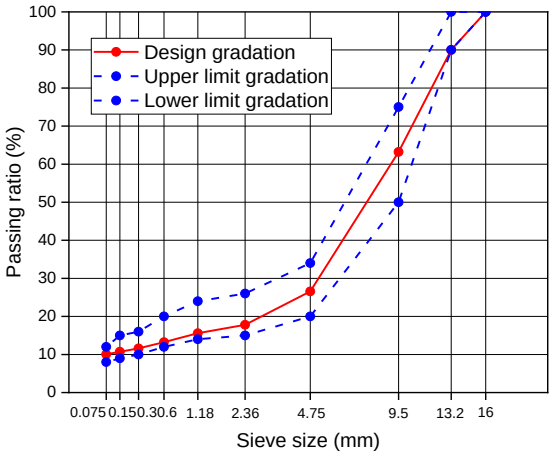

Figure 1. Aggregate gradations of SMA-13.

3.2. Filler Test Methods

3.2.1. Particle Size Test

A laser particle size analyzer (Hydro 2000MU) was used to determine the particle size distributions of the fillers. The testing size ranges were set at 0.01–300 μm. The collected data allowed the calculation of the Sauter mean diameter (D[3,2]) according to Equation (1):

$$D_{[3,2]} = \frac{\sum_i n_i D_i^3}{\sum_i n_i D_i^2} \quad (1)$$

where n_i is the droplet number and D_i is the ith particle diameter.

3.2.2. Environmental Scanning Electron Microscope (ESEM) Test

An environmental scanning electron microscope was adopted to observe the micro-surface characteristics of the investigated fillers. The microscope images were magnified from 200 to 600 times.

3.3. Mastic Test Methods

3.3.1. Steady Shear Viscosity Test

A steady shear viscosity test was conducted at 64 °C with a shear rate ranging from 0.001 s^{-1} to 1 s^{-1}. Based on the Carreau–Yasuda model (Equation (2)), the shear viscosity was used to calculate ZSV [22].

$$\frac{\eta - \eta_\infty}{\eta_0 - \eta_\infty} = \left[1 + (\lambda\dot{\gamma})^a\right]^{(n-1)/a} \quad (2)$$

where η is the mastic viscosity (Pa·s); η_0 is the zero shear viscosity (Pa·s); η_∞ is the infinite shear viscosity (Pa·s); $\dot{\gamma}$ is the shear rate (s^{-1}); and λ, n, and a are the shape parameters.

3.3.2. Multiple-Stress Creep Recovery (MSCR) Test

Following AASHTO TP 70-12 [27], the multiple-stress creep recovery test was performed at 64 °C to evaluate the high-temperature properties of the five asphalt mastics. Repeated cycles of creep and recovery were applied to samples at two stress levels (0.1 kPa and 3.2 kPa). The non-recoverable creep compliance (J_{nr}) and the average strain recovery (R) values were calculated according to Equations (3) and (4) [27], respectively, to determine the viscoelastic behavior of the mastics.

$$R_{0.1/3.2} = \sum((\varepsilon_1 - \varepsilon_{10})/\varepsilon_1)/10 \quad (3)$$

$$J_{nr0.1/3.2} = \sum(\varepsilon_{10}/\tau)/10 \quad (4)$$

where ε_1 is the strain value for each cycle at 1 s, ε_{10} is the strain value for each cycle at 10 s, and τ is the applied shear stress loading.

As a viscoelastic multiphase material, asphalt mastic is composed of a viscoelastic matrix and elastic solid aggregates. Therefore, we applied the Burgers four-element model [28] to express the creep and recovery responses in the MSCR tests. In general, the Burgers model consists of the Maxwell unit (separate dashpot and spring elements) and the Kelvin unit (combined dashpot and spring element) (Figure 2).

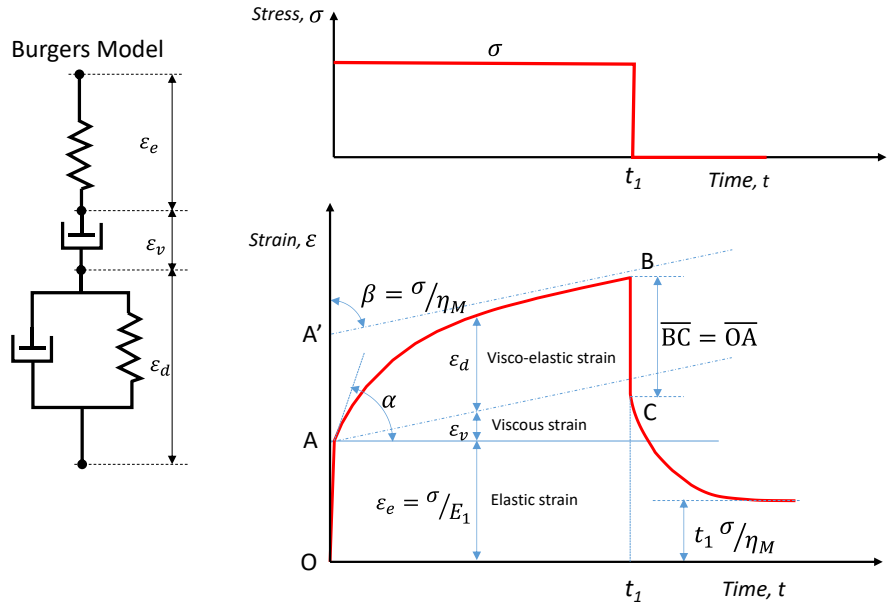

Figure 2. Strain response of Burgers model.

Correspondingly, the total strain under loading of the asphalt included three components: elastic, delayed, and viscous strain. Equation (5) describes the constitutive Burgers model:

$$\varepsilon(t) = \varepsilon_e + \varepsilon_v + \varepsilon_d = \frac{\sigma}{E_M} + \frac{\int \sigma(t)dt}{\eta_M} + \left(\frac{1}{\eta_K}\int \sigma(t)e^{\frac{E_K}{\eta_K}t}dt\right)e^{-\frac{E_K}{\eta_K}t} \quad (5)$$

where ε and σ are strain and stress, respectively; t is the loading time; ε_e, ε_v, and ε_d are the elastic, viscous, and delayed elastic strain, respectively; E_M and η_M are the moduli of the spring and the viscosity of the dashpot in Maxwell units, respectively; and E_K and η_K are the moduli of the spring and the viscosity of the dashpot in Kelvin units, respectively.

3.3.3. Linear Amplitude Sweep (LAS) Test

Following AASHTO TP 101-12 [29], a linear amplitude sweep test was conducted at 25 °C to evaluate the fatigue performance of the asphalt mastics. The frequency sweep test was first applied from 0.2 Hz to 30 Hz at a constant strain amplitude of 0.1%; then, the shear strain was linearly increased from 0.1% to 30% at 10 Hz. The failure state of damage accumulation was defined as a 35% reduction in the initial modulus, based on the viscoelastic continuum damage (VECD) theory [30].

3.3.4. Time Sweep Test

Time sweep tests were performed to investigate the fatigue resistance of the asphalt mastics in the stress-controlled mode. All the tests were conducted at 25 °C with a stress

amplitude of 100 kPa. A 50% reduction in the initial stiffness or dynamic shear modulus of a material is commonly defined as fatigue failure (Equation (6)):

$$S = \frac{|G*|}{|G*|_{Initial}} \tag{6}$$

where S is the dynamic shear modulus ratio and $|G*|$ is the dynamic shear modulus.

Additionally, the $S \times N$ peak was calculated to determine the fatigue life of the asphalt materials, where N is the loading cycle number [30].

3.4. Mixture Test Methods

3.4.1. Wheel-Tracking Test

Wheel-tracking tests were conducted at 60 °C and 0.7 MPa to evaluate the rutting performance at a high temperature according to Equation (7):

$$DS = \frac{(60 - 45) \times N}{d_{60} - d_{45}} \tag{7}$$

where DS is the dynamic stability of the mixture (time/mm); N is the test wheel round-trip rolling speed, which is usually 42 (time/min); and d_{60} and d_{45} are the concavity depths of the experimental car after driving for 60 min and 45 min, respectively (mm).

3.4.2. Dynamic Creep Test

Following NCHRP Report 465 [31], the dynamic creep test was performed on cylindrical specimens to evaluate the high-temperature fatigue of the asphalt mixtures. This test used a half-sinusoidal pressure load for single-axis dynamic repetitive loading with a 0.1 s loading time and a 0.9 s intermittent time. The axial pressure was set to 100 kPa at 64 °C. Cylindrical specimens formed by a rotary compactor with a diameter of 100 mm and a height of 150 mm were used for the test (Figure 3a). The void ratio of all the specimens was controlled at 4 ± 0.5%. During the test, the permanent deformation of the asphalt mixture was recorded as a function of the number of load repetitions [32], generally comprising three stages:

1. Initial stage (migration period, fatigue cracking): the permanent strain increased rapidly, but the strain rate gradually decreased;
2. Second stage (stable period, crack expansion): the permanent strain grew steadily, and the strain rate remained unchanged;
3. Third stage (destruction period, structural failure): the permanent strain and strain rate increased sharply, and shear flow occurred until the specimen was destroyed.

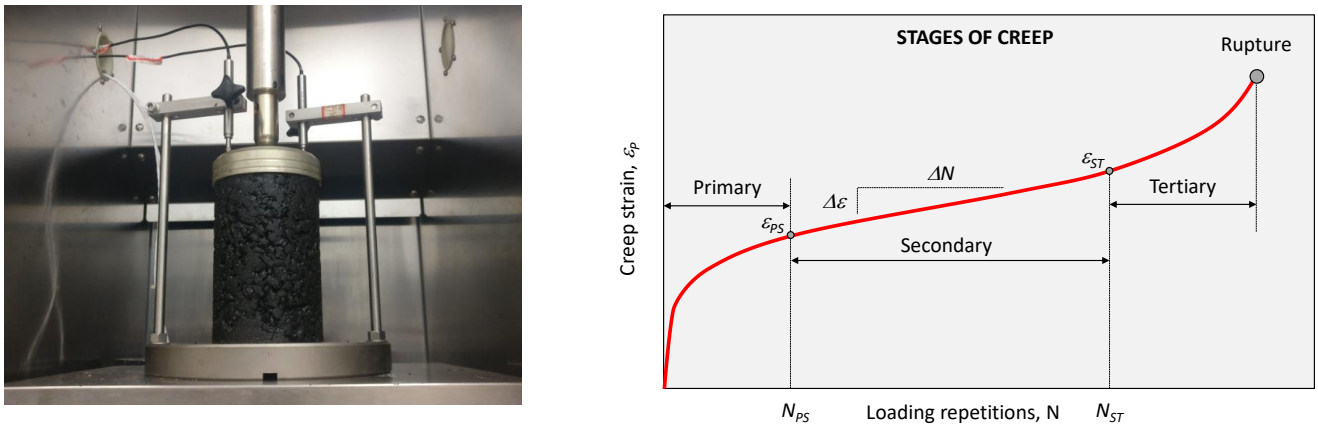

(**a**) (**b**)

Figure 3. Dynamic creep test process: (**a**) testing device; (**b**) typical creep stages.

The results of the dynamic creep test were analyzed based on the three-stage model (Figure 3b) described by Equations (8)–(10) [32]:

$$\varepsilon_p = aN^b, N < N_{PS} \quad (8)$$

$$\varepsilon_p = \varepsilon_{PS} + c(N - N_{PS}), N_{PS} \leq N < N_{ST} \quad (9)$$

$$\varepsilon_p = \varepsilon_{ST} + d\left(e^{f(N-N_{st})} - 1\right), N \geq N_{ST} \quad (10)$$

where ε_p is the permanent strain; N is the number of repetitions; a, b, c, d, and f are fitting coefficients; N_{PS} is the load number corresponding to the initial point of the second stage (i.e., the endpoint of the first stage); ε_{PS} is the permanent strain corresponding to the initial point of the second stage; and N_{ST} and ε_{ST} are the load number corresponding to the initial point of the third stage (i.e., the endpoint of the second stage) and the permanent strain corresponding to the initial point of the third stage, respectively.

4. Results and Discussion

4.1. Microscopic Characteristics of Fillers

4.1.1. Particle Size Distribution

Figure 4 shows the particle size distributions of the LF and MSWI residues, and Table 4 lists the monitored grading indicators. The average particle diameter, the particle diameter of the 50th cumulative mass percentile (D50), the peak size, and the peak intensity were calculated.

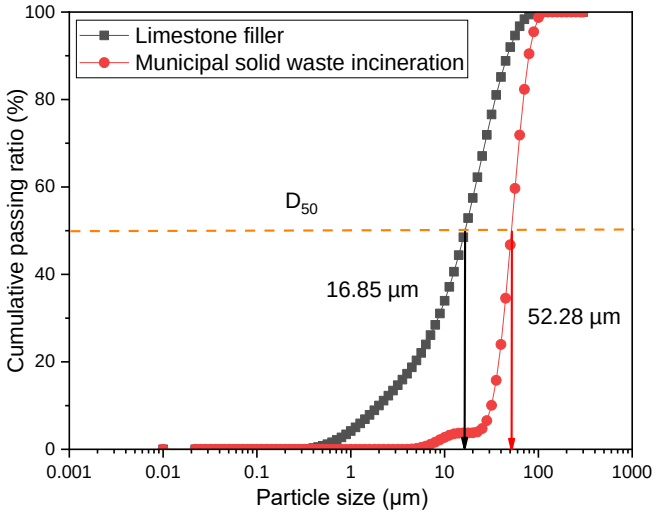

Figure 4. Particle size distribution of fillers.

Table 4. LF and MSWI residue particle size distribution indicators.

Indicator	LF	MSWI
Average particle diameter (μm)	20.96	53.30
D_{50} (μm)	16.85	52.28
Peak size (μm)	25.18	56.37
Peak intensity (%)	4.84	12.88
$D_{[3,2]}$ (μm)	49.95	70.24

As shown in Figure 4, the cumulative passing percentage of the MSWI residue increased rapidly for a larger particle size range. The larger cumulative passing ratio of the MSWI residue corresponded to a lower specific surface area than the LF, which indicated a

smaller contact area with the bitumen. The differences in the accumulative passing ratio between the MSWI residue and LF would increase the system inhomogeneity and affect the interface interactions between the bitumen and filler.

Figure 4 and Table 4 show that the MSWI residue comprised larger particles with a more concentrated distribution than the LF.

4.1.2. Microsurface Morphology

ESEM images magnified 200 and 600 times allowed the characterization of the microsurface and -structure of the LF and MSWI residue (Figure 5a–d).

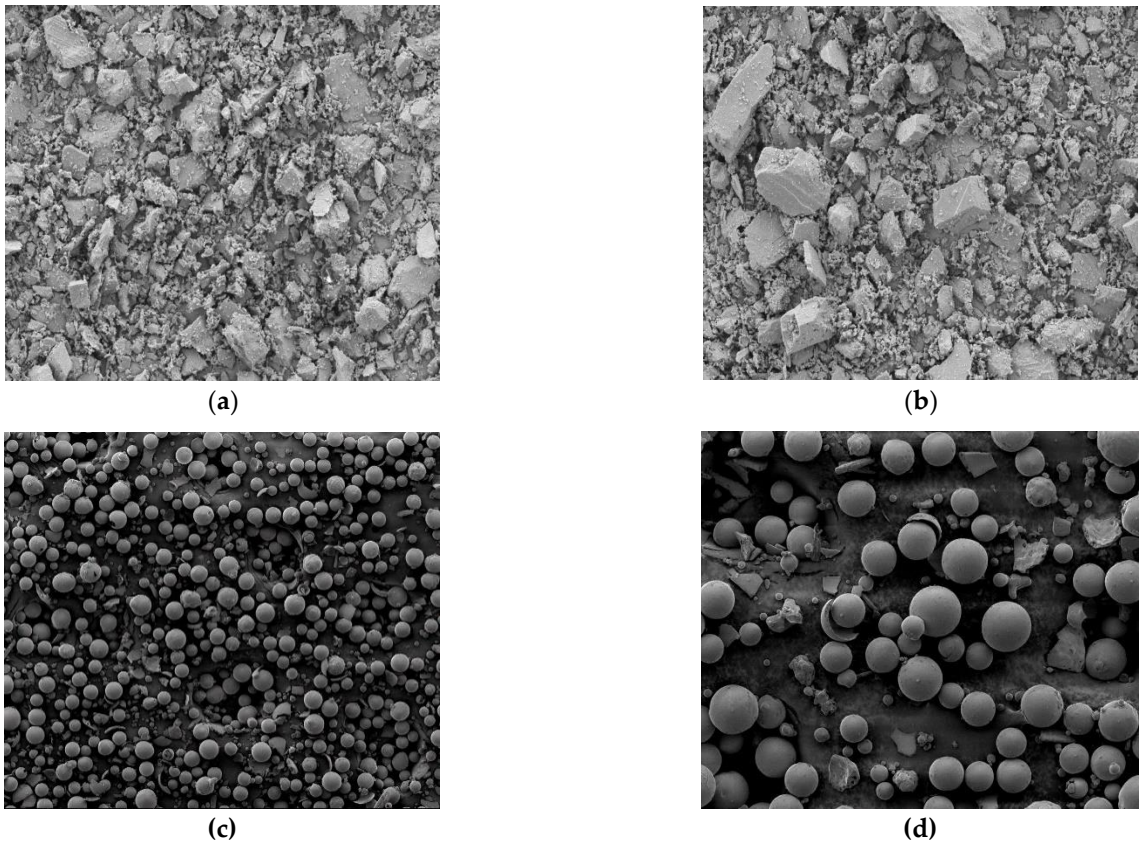

Figure 5. ESEM images of (**a**) LF magnified 200 times; (**b**) LF magnified 600 times; (**c**) MSWI residue magnified 200 times; (**d**) MSWI residue magnified 600 times.

The two fillers presented different surface morphologies and microtextures. The particle shapes of the LF were irregular, with discontinuities and pores that contributed to a higher specific surface area and enhanced its absorption properties. By contrast, the majority of the MSWI residue particles exhibited a homogenous distribution and spherical shapes. Additionally, the relatively smooth surface of the MSWI residue particles resulted in poorer absorption. We inferred that the MSWI residue had a smaller specific surface area and contact area with the bitumen than the LF. Therefore, the microscopic characteristics of the fillers affected the engineering properties of the asphalt mastics and mixtures.

4.2. High-Temperature Performance

4.2.1. Zero-Shear Viscosity of Mastics

Figure 6a presents the complex viscosity curves of the five asphalt mastics at 64 °C, and Figure 6b shows their shear viscosity values.

Figure 6a demonstrates that all the asphalt mastics entered the first Newton region at low angular frequencies (from 1×10^{-5} to 0.001 rad/s) and behaved as Newton liquids, with the viscosity exhibiting very small variations (from 3437 to 1869 Pa·s). For Figure 6a,

the Carreau–Yasuda model (Equation (1)) was adopted to calculate the zero- and infinite-shear viscosities of the asphalt mastics. Both η_0 and η_∞ decreased with the MSWI residue content (Figure 6b). However, the range of variation in the complex viscosity with a higher MSWI residue content was smaller under a shear frequency (Figure 6a). The trend of η_∞ values among the asphalt mastics corresponded with the results of the ZSV, because the MSWI residue increased the viscous component of the asphalt mastics and reduced their stiffness.

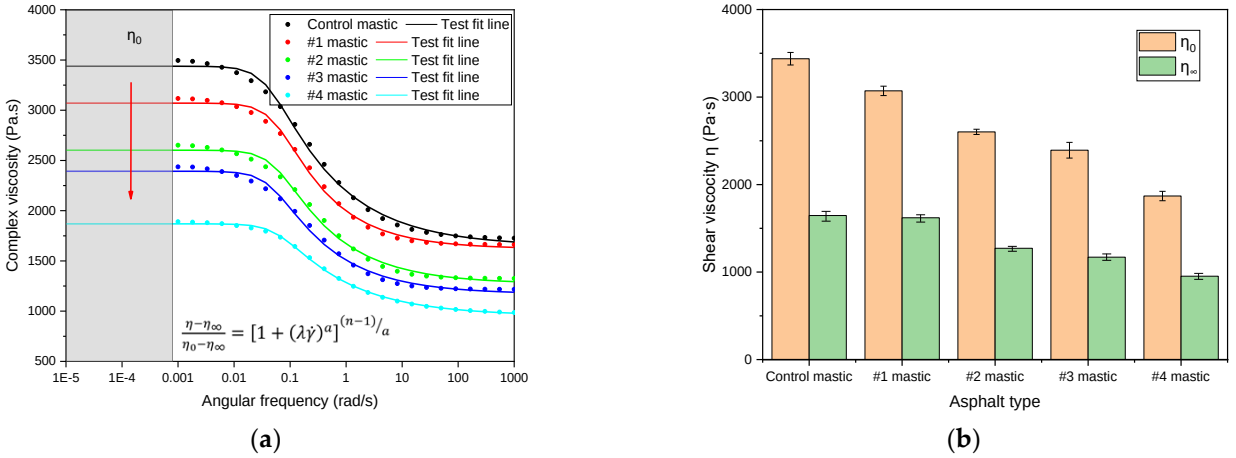

Figure 6. Results of the steady shear viscosity tests: (**a**) viscosity–frequency curve, and (**b**) shear viscosity.

4.2.2. Viscoelastic Characteristics of Mastics

Figure 7a,b show the shear strain variations over time in the MSCR tests at 0.1 kPa and 3.2 kPa, respectively. Because the filler-to-asphalt ratio (i.e., 1.2) was kept the same, the shear strain curves exhibited similar variations over time for all the asphalt mastics. However, the addition of the MSWI residue increased the range and rate of shear strain significantly compared with the control mastic. Therefore, the inclusion of MSWI residue in asphalt mastic reduced the resistance to deformation.

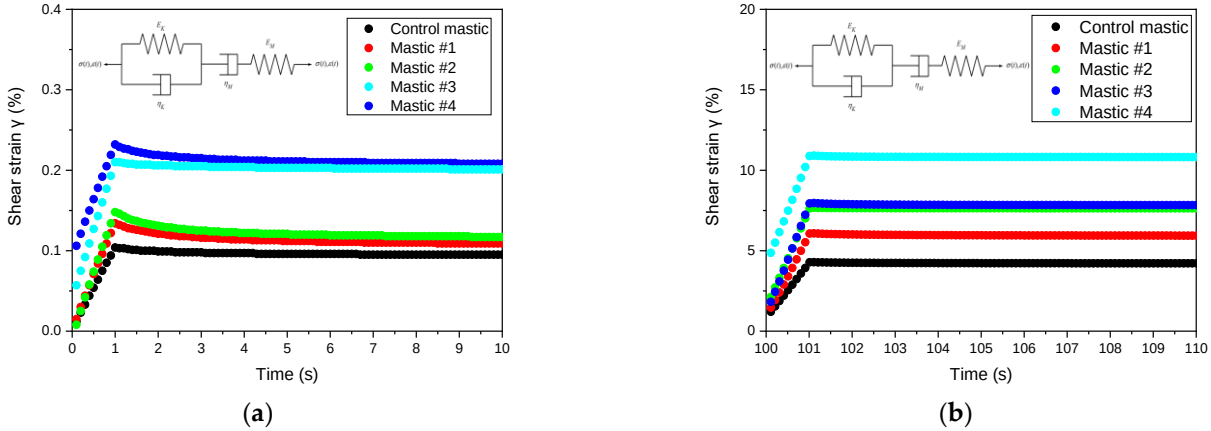

Figure 7. Shear strain variations over time in MSCR tests: (**a**) 0.1 kPa; (**b**) 3.2 kPa.

Table 5 lists the fitting parameters of the Burgers models for the investigated asphalt mastics.

Replacing LF with MSWI residue reduced the spring modulus and dashpot viscosity in the Burgers models at both low and high stress levels. The fitting results of the Burgers models also indicated that the asphalt mastic with the highest MSWI residue content exhibited the worst resistance to permanent deformation.

Table 5. Fitting parameters of Burgers models.

Variable	Unit	Control Mastic	Mastic #1	Mastic #2	Mastic #3	Mastic #4
$E_{M0.1}$	Pa	1094.47	1079.59	1077.56	1055.86	1055.50
$\eta_{M0.1}$	Pa·s	33.12	28.12	26.09	15.76	15.13
$E_{K0.1}$	Pa	569.10	326.44	300.30	163.14	62.9
$E_{M3.2}$	Pa	11.91	10.95	8.70	6.22	1.82
$\eta_{M3.2}$	Pa·s	0.75	0.53	0.42	0.40	0.29
$E_{K3.2}$	Pa	23.19	22.93	22.06	21.85	21.08

4.2.3. Rutting Resistance of Mixtures

Figure 8 shows the results of the wheel-tracking test performed to evaluate the rutting resistance of the five asphalt mixtures. The dynamic stability (DS) of the mixtures decreased with an increase in the MSWI residue content from 8873.2 cycles/mm in the control mixture to 3937.5 cycles/mm in mastic #4. However, all the DS values passed the minimum requirement (3000 cycles/mm) provided by the technical specification (JTG F40-2004) [33]. Although the replacement of LF with MSWI residue reduced the rutting resistance, the MSWI residue asphalt mixtures met the basic anti-rutting performance requirements for flexible pavements.

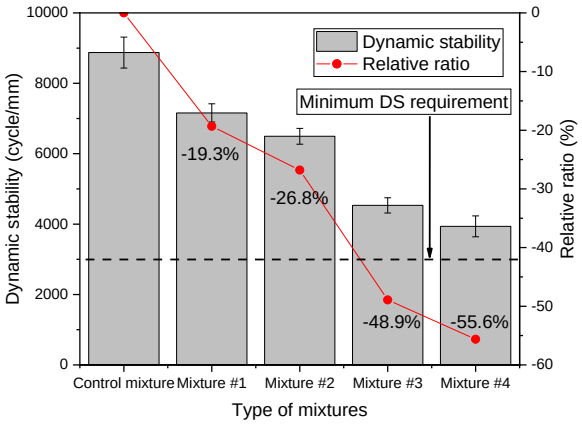

Figure 8. Wheel-tracking test results.

The low absorbability of the MSWI residue in the asphalt mastic was one of the main reasons for the decrease in rutting resistance. This was because the smooth surface of the MSWI residue particles reduced the interfacial bonding and resulted in the nonuniform distribution of stress between the bitumen and MSWI residue, decreasing the rutting resistance.

4.3. Fatigue Properties

4.3.1. LAS Analysis of Mastics

Following AASHTO TP 101-12 [29], Table 6 lists the fitting parameters for the fatigue life prediction models of the investigated asphalt mastics. A_{35} and B represent the damage characteristic parameters with dimensionless units. The equations for fatigue life prediction in Table 6 were based on the VECD theory and provide the number of loads (N_f) corresponding to ε_p = 5%.

Figure 9 shows the fatigue life prediction results for different MSWI residue contents (from 0% to 100%) and shear strains (from 1% to 10%). For a given MSWI residue content, the fatigue life of the mastics reduced rapidly with an increasing strain level from 1% to 10%, and the asphalt mastics became damaged [34]. Additionally, for a constant strain level, the fatigue life decreased with an increasing MSWI residue content. We inferred that the nonuniform distribution of stress between the bitumen and MSWI residue increased

the stress sensitivity of the mastics, reducing the fatigue resistance of the mixtures [35,36]. Therefore, the MSWI residue content significantly affected the behavior of HMA [37].

Table 6. Fitting parameters and fatigue life prediction models.

Asphalt Type	$A_{35}/10^{7}$ [1]	B [1]	Fatigue Prediction Equation
Control mastic	4.869	4.738	$N_f = 4.869 \times 10^8 (\gamma_{max})^{-4.738}$
Mastic #1	3.895	4.764	$N_f = 3.895 \times 10^8 (\gamma_{max})^{-4.764}$
Mastic #2	2.301	4.728	$N_f = 2.301 \times 10^8 (\gamma_{max})^{-4.728}$
Mastic #3	2.173	4.730	$N_f = 2.173 \times 10^8 (\gamma_{max})^{-4.730}$
Mastic #4	1.000	4.842	$N_f = 1.000 \times 10^8 (\gamma_{max})^{-4.842}$

[1] A_{35} and B represent the fitting parameters with dimensionless units.

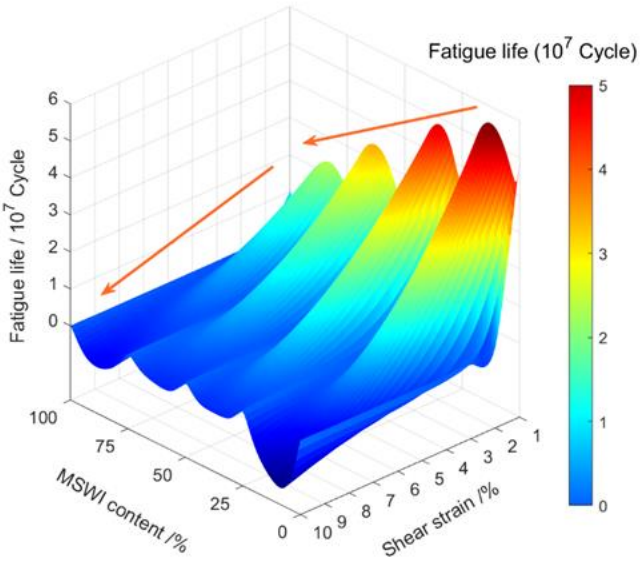

Figure 9. Fatigue life prediction.

Figure 10a,b represent the fatigue life of the five asphalt mastics at two strain levels (2.5% and 5%, respectively). The fatigue life of the asphalt mastics decreased significantly by over 52.1% when the MSWI residue content reached 50%. The total replacement of the LF with MSWI residue in the asphalt mastic reduced the fatigue life by over 81.3%. Therefore, the reuse of MSWI residues in asphalt mastics requires detailed investigations to control its negative effects on the fatigue and durability performance of asphalt materials.

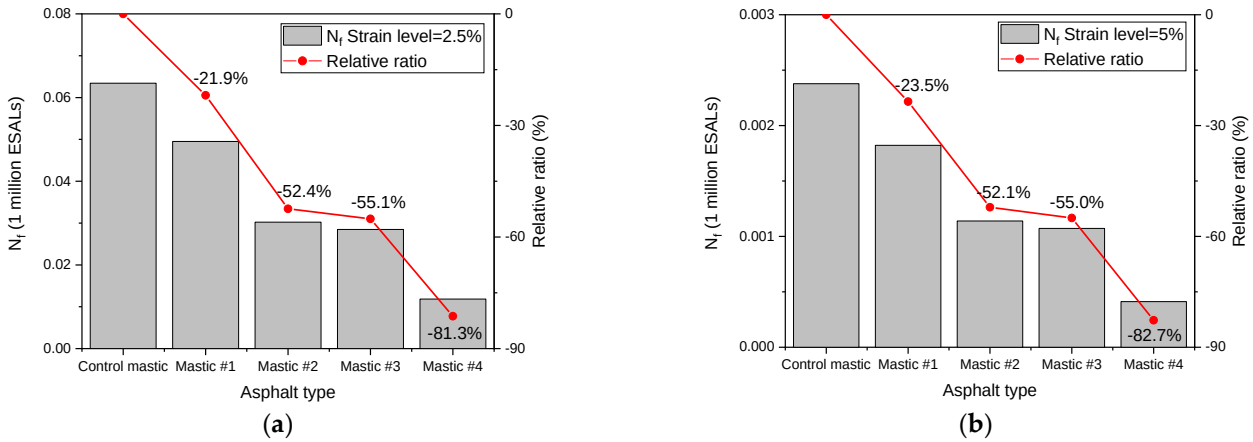

Figure 10. Fatigue life: (**a**) strain level = 2.5%, (**b**) strain level = 5%.

4.3.2. Time Sweep Analysis of Mastics

The fatigue life was defined as the loading cycle number corresponding to the S × N maximum value. Therefore, two principles were followed to evaluate the fatigue resistance of the mastics. Figure 11a,b present the dynamic shear modulus ratio and S × N peak versus the cycle number for the asphalt mastics, respectively.

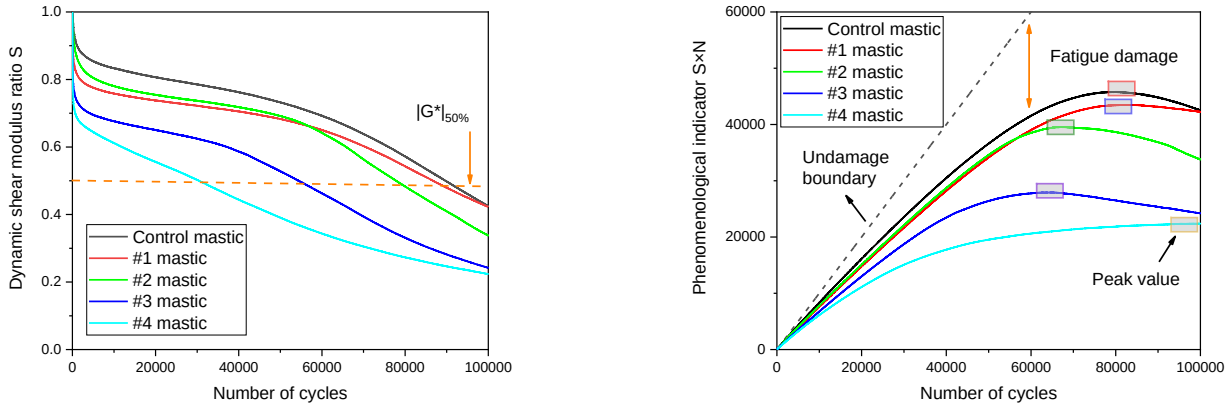

Figure 11. Time sweep analysis: (**a**) S curve; (**b**) S × N curve.

As shown in Figure 11a, the S values decreased gradually as the cycle number increased. Similarly, the S × N curves in Figure 11b diverged from the undamaged boundary and continuously declined after the peak, which indicated fatigue failure occurrence. Figure 12 shows the number of cycles until fatigue for the asphalt mastics. The fatigue life reduced from the control mastic to Mastic #4 due to the addition of MSWI residue. The fatigue life predictions for all samples were consistent, except for a slight deviation in the value of Mastic #4 due to the criterion of the S × N peak. This failure criterion became invalid when the descending speed of the S curve decreased, which resulted in a significant delay in the S × N peak emergence.

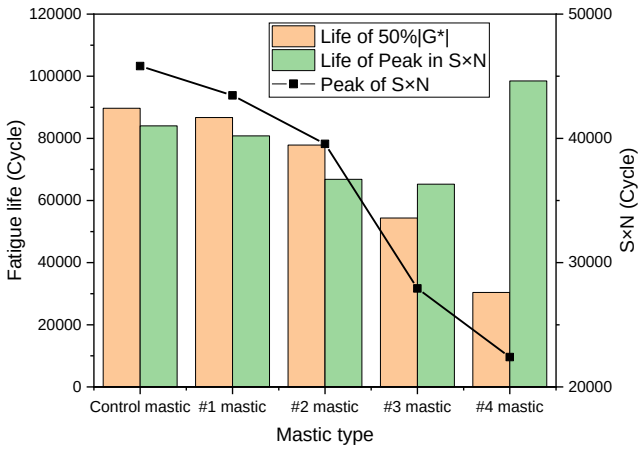

Figure 12. Fatigue life evaluation according to the two failure criteria.

4.3.3. Dynamic Creep Analysis of Mixtures

Based on the viscoelastic properties of the asphalt mixture, a dynamic creep test was applied to simulate the dynamic response of a pavement under different loads and environmental conditions. Figure 13 shows the permanent deformation curves of the considered asphalt mixtures, and Table 7 lists the fitting parameters of the permanent deformation curves according to Equations (8)–(10). In Figure 13, N_f is the number of cycles corresponding to a strain ε_p = 5%.

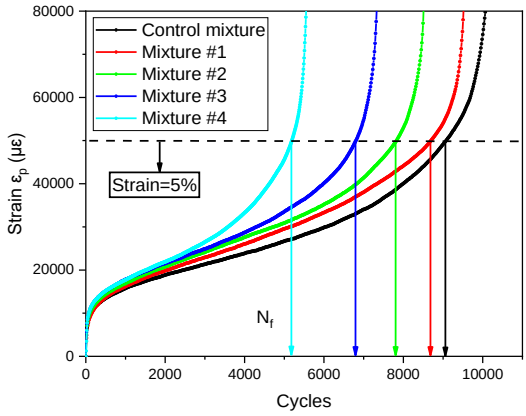

Figure 13. Permanent deformation curves.

Table 7. Three-stage model fitting parameters of permanent deformation curves.

Parameter	Control Mixture	Mixture #1	Mixture #2	Mixture #3	Mixture #4
N_f	9089	8705	7829	6812	5193
a	2881.9	2457.7	2979	3450.9	3204.3
b	0.2468	0.2743	0.2529	0.2380	0.2493
N_{PS} (cycles)	2545	2273	1764	1700	1645
ε_{PS} (με)	20,160	20,627	19,920	20,460	20,513
c	2.7518	3.3169	3.5829	3.6967	4.5275
N_{ST} (cycles)	6001	5841	5473	4724	3284
ε_{ST} (με)	29,880	32,623	32,747	31,927	27,993

As shown in Table 7, only N_{PS}, c, and N_{ST} presented significant change trends. However, N_{PS} was not selected as an evaluation index, because it overlooked the results after the first stage. Conversely, N_{ST} represented the starting point of the asphalt mixture entering the shear flow deformation stage (flow number, F_n) and c represented the creep rate ($\varepsilon_p$slope) [38].

The permanent deformation and the creep rate curves in Figure 14 complied with the data in Table 7.

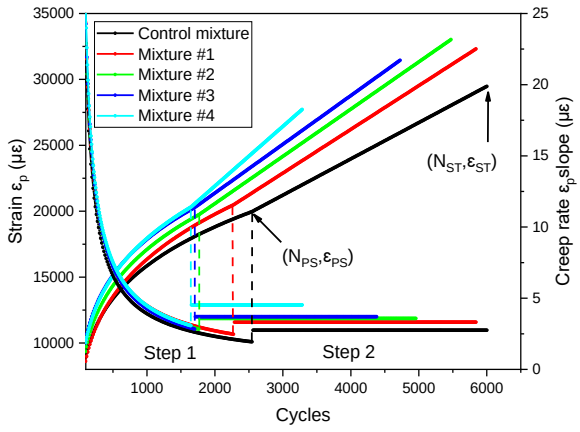

Figure 14. Permanent deformation and creep rate.

In addition to the above indicators, the flow index F_i (i.e., the ratio of the permanent strain ε_p to the F_n) and N_f were used to evaluate the anti-rutting performance of the asphalt mixtures. The smaller the F_i value, the stronger the resistance to deformation, while F_i comprehensively measured the void ratio of the mixtures and the resistance to shear loads, to some extent [39,40].

Based on the flow number test, four indicators (F_n, N_f, F_i, and $\varepsilon_p$slope) were selected to interpret the high-temperature performance of the asphalt mixtures (Figures 15 and 16). In Figures 15 and 16, the ratios of the four indicators are defined as the ratios of increase or decrease compared to the control mixture.

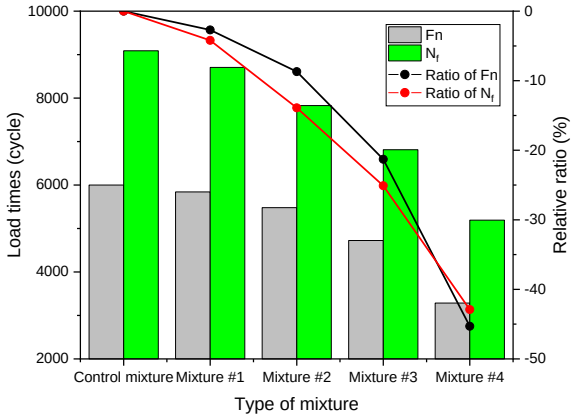

Figure 15. Flow number and number of failures.

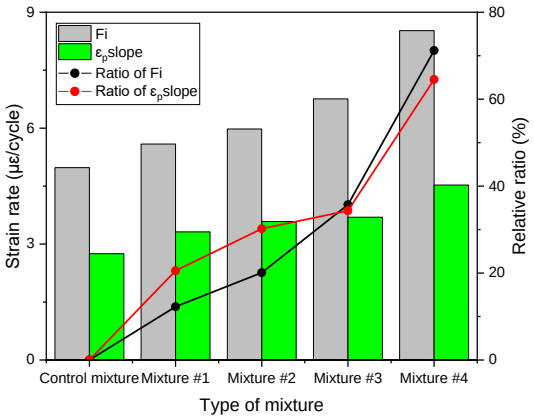

Figure 16. Flow number index and creep rate.

The control mixture had a much higher F_n (6001 cycles) than mixture #4 (3284 cycles), so the mixtures with MSWI residue entered the shear flow deformation stage sooner. Similarly, mixture #4 had the lowest N_f (i.e., 5193), which confirmed its poorer anti-fatigue ability according to the DSR tests of the asphalt mastics. Moreover, the addition of MSWI residue caused a rising trend in the F_i and $\varepsilon_p$slope, which presented increased ratios of 71.2% and 64.5%, respectively. Therefore, the flow number test confirmed that MSWI residue significantly reduced the high-temperature fatigue performance of the asphalt mixtures.

5. Statistical Analyses

According to the experimental results, the high-temperature rheological and fatigue characteristics of the tested materials declined with a higher MSWI residue content. The measured parameters were compared pairwise between the asphalt mastic and mixture properties by calculating the Pearson correlation coefficient (R). Regarding the rheological properties, Figure 17a–c show the correlation curves between dynamic stability and shear viscosity, dynamic stability and the parameters of the Burgers model at 0.1 kPa, and dynamic stability and the parameters of the Burgers model at 3.2 kPa, respectively.

Regarding the fatigue properties of the asphalt mastics and mixtures, Figure 18a to c show the correlation curves between A_{35} and the load number, the fatigue life of 50% $|G*|$ and the load number, and the peak value of S × N and the load number, respectively.

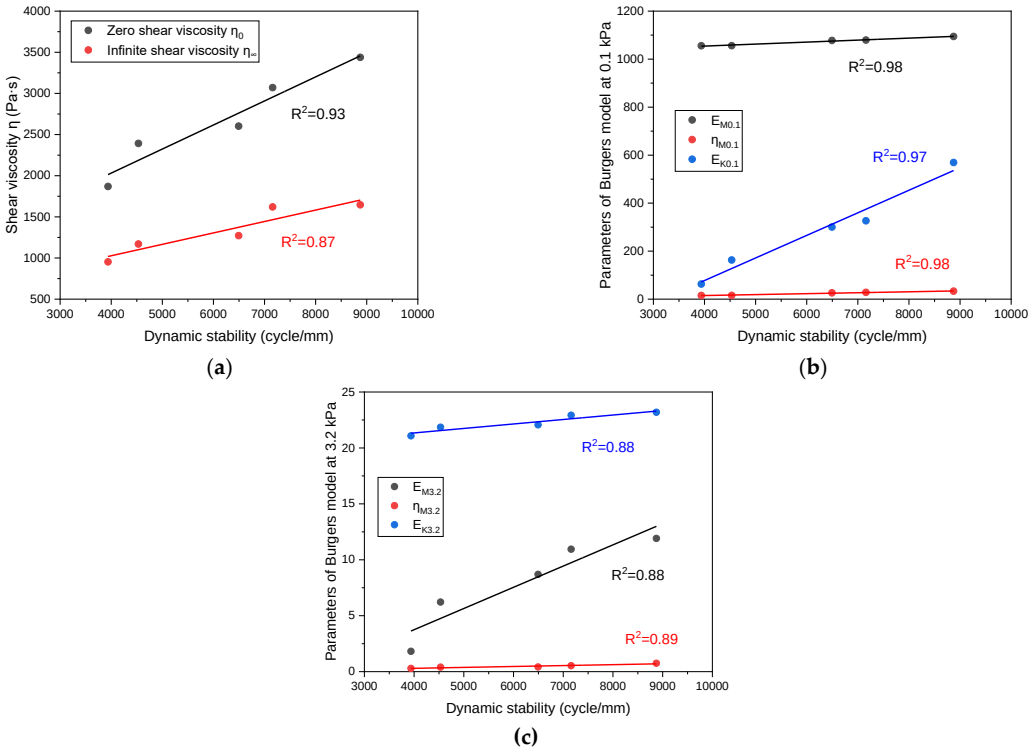

Figure 17. Correlation analysis of the rheological properties of the mastics and mixtures: (**a**) dynamic stability and shear viscosity; (**b**) dynamic stability and parameters of the Burgers model at 0.1 kPa; (**c**) dynamic stability and parameters of the Burgers model at 3.2 kPa.

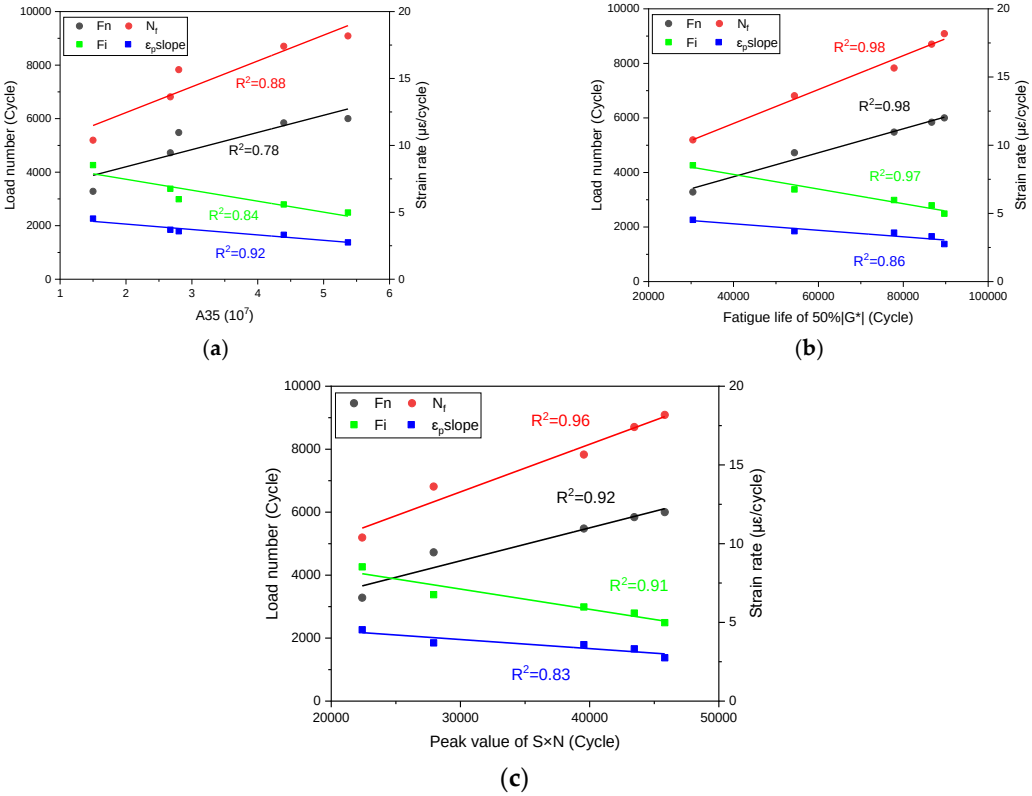

Figure 18. Correlation analysis of the fatigue properties of mastics and mixtures: (**a**) A_{35} and load number; (**b**) fatigue life of 50% |G∗| and load number; (**c**) peak value of S × N and load number.

According to Figures 17 and 18, the investigated parameters were significantly correlated (R^2 no less than 0.78) between the asphalt mastics and mixtures. Therefore, the asphalt mastics were reliable materials to predict the high-temperature rheological and fatigue performance of the corresponding mixtures. Moreover, the correlations between the performance indices further verified the asphalt materials' rutting and fatigue resistance.

6. Conclusions

The growing awareness of sustainability has encouraged the recycling and reuse of MSWI residues in road construction, whose purpose is to mitigate the problems of stockpiling these materials in cities and decrease the associated environmental burden and construction costs. When studying the applications of MSWI residue, one should follow the general principle of maintaining a careful balance between engineering performance and economic/environmental benefits. In this study, MSWI residue, which is a by-product of waste combustion in thermal power plants, was used as an alternative material to replace 0% to 100% of the natural mineral filler in five asphalt mastics and five mixtures. PG 64-22 bitumen was used for sample preparation. All the tested asphalt mixtures were SMA-13. Based on the test results, we drew the following main conclusions:

- The low absorbability of MSWI residue in asphalt mastic stemmed from its morphological characteristics of hollow, spherical particles with smooth surfaces, which affected the rheological and fatigue characteristics of the mixtures;
- The replacement of LF with MSWI residue reduced the elastic and viscous components in the asphalt mastics. However, the dynamic stability of all the tested mixtures was above 3000 cycle/mm, meeting the minimum requirements of the specifications and providing a basic level of rutting resistance;
- Regardless of the failure criterion adopted, the fatigue life predictions for the asphalt mastics decreased by more than 42.9% according to the MSWI residue/LF volume ratio, demonstrating the negative effect of MSWI residue incorporation on fatigue resistance;
- The three-stage model described the permanent deformation of the asphalt mixtures. The flow number test also confirmed that MSWI residue reduced the high-temperature fatigue performance of the asphalt mixtures;
- Significant correlations were found between the performance parameters of the asphalt mastics and mixtures in terms of rheological and fatigue properties. The correlation coefficients (R^2) between the rheological and fatigue properties of the mastics and mixtures were over 0.87 and 0.78, respectively. These regressions could be used in the asphalt mixture design process to establish the correct proportion of alternative materials with regard to the expected performance;
- The rheological and fatigue characteristics of the mixtures revealed both the potential and limitations of using MSWI residues in flexible pavements. The use of MSWI residues in asphalt mixtures still requires in-depth consideration and investigation before implementation, despite the technological developments in the incorporation of MSWI residues with inorganic materials.

Based on the above, we offer several suggestions for further studies:

(1) The low absorbability of the MSWI residue was a limitation of this study. Therefore, surface treatments and coupling modifiers are suggested for future research to enhance the microstructural properties of MSWI residues and their interaction with bitumen;
(2) In most cases, the use of MSWI residues does not pose a threat to human health; however, in the worst-case scenario, the heavy metals within MSWI residues might cause water or soil contamination. Future studies should focus on leaching investigations and the origins of leachates to prevent any side effects of employing MSWI residues;
(3) Life-cycle assessment (LCA) and life-cycle cost analysis (LCCA) should be conducted to evaluate the environmental and economic effects of reusing MSWI residues in asphalt mixtures over their entire service life. The objective assessment of pollution mitigation could favor recycling and reusing MSWI residues.

Author Contributions: Conceptualization, L.X. and Y.D.; methodology, L.X. and Y.D.; software, L.X. and Y.D.; validation, L.M. and G.L.; formal analysis, Y.D. and L.M.; investigation, L.X., L.M. and G.L.; resources, Y.D.; data curation, L.X.; writing-original draft preparation, L.X.; writing—review and editing, G.L. and L.M.; visualization, L.X.; supervision, Y.D.; project administration, Y.D.; funding acquisition, Y.D. and G.L. All authors have read and agreed to the published version of the manuscript.

Funding: This research was funded by the National Natural Science Foundation of China (Grant number 51808562), Natural Science Foundation of Hunan Province, China (Grant number 2020JJ5723) and within the grant number RM120172B05C0B39, financed by the Sapienza, University of Rome.

Institutional Review Board Statement: Not applicable.

Informed Consent Statement: Not applicable.

Data Availability Statement: The data presented in this study are available on request from the corresponding author.

Conflicts of Interest: The authors declare no conflict of interest.

References

1. Moretti, L.; Loprencipe, G. Climate Change and Transport Infrastructures: State of the Art. *Sustainability* **2018**, *10*, 4098. [CrossRef]
2. Dou, X.; Ren, F.; Nguyen, M.Q.; Ahamed, A.; Yin, K.; Chan, W.P.; Chang, V.W.-C. Review of MSWI bottom ash utilization from perspectives of collective characterization, treatment and existing application. *Renew. Sustain. Energy Rev.* **2017**, *79*, 24–38. [CrossRef]
3. Abbà, A.; Collivignarelli, M.C.; Sorlini, S.; Bruggi, M. On the reliability of reusing bottom ash from municipal solid waste incineration as aggregate in concrete. *Compos. Part B Eng.* **2014**, *58*, 502–509. [CrossRef]
4. Muangrat, R. A review: Utilization of food wastes for hydrogen production under hydrothermal gasification. *Environ. Technol. Rev.* **2013**, *2*, 85–100. [CrossRef]
5. Nahman, A.; de Lange, W.; Oelofse, S.; Godfrey, L. The costs of household food waste in South Africa. *Waste Manag.* **2012**, *32*, 2147–2153. [CrossRef] [PubMed]
6. Okajima, I.; Sako, T. Energy conversion of biomass with supercritical and subcritical water using large-scale plants. *J. Biosci. Bioeng.* **2014**, *117*, 1–9. [CrossRef]
7. Roessler, J.G.; Townsend, T.G.; Ferraro, C.C. Use of leaching tests to quantify trace element release from waste to energy bottom ash amended pavements. *J. Hazard. Mater.* **2015**, *300*, 830–837. [CrossRef]
8. Allegrini, E.; Vadenbo, C.; Boldrin, A.; Astrup, T.F. Life cycle assessment of resource recovery from municipal solid waste incineration bottom ash. *J. Environ. Manag.* **2015**, *151*, 132–143. [CrossRef]
9. del Valle-Zermeño, R.; Formosa, J.; Chimenos, J.M.; Martínez, M.; Fernández, A.I. Aggregate material formulated with MSWI bottom ash and APC fly ash for use as secondary building material. *Waste Manag.* **2013**, *33*, 621–627. [CrossRef]
10. Luo, H.-L.; Chen, S.-H.; Lin, D.-F.; Cai, X.-R. Use of incinerator bottom ash in open-graded asphalt concrete. *Constr. Build. Mater.* **2017**, *149*, 497–506. [CrossRef]
11. Lynn, C.J.; Ghataora, G.S.; Dhir OBE, R.K. Municipal incinerated bottom ash (MIBA) characteristics and potential for use in road pavements. *Int. J. Pavement Res. Technol.* **2017**, *10*, 185–201. [CrossRef]
12. Aysen Lav, M.; Hilmi Lav, A. Effects of stabilization on resilient characteristics of fly ash as pavement material. *Constr. Build. Mater.* **2014**, *54*, 10–16. [CrossRef]
13. Stabile, P.; Bello, M.; Petrelli, M.; Paris, E.; Carroll, M.R. Vitrification treatment of municipal solid waste bottom ash. *Waste Manag.* **2019**, *95*, 250–258. [CrossRef] [PubMed]
14. O'Donnell, S.T.; Caldwell, M.D.; Barlaz, M.A.; Morris, J.W.F. Case study comparison of functional vs. organic stability approaches for assessing threat potential at closed landfills in the USA. *Waste Manag.* **2018**, *75*, 415–426. [CrossRef]
15. Chang, N.-B.; Wang, H.P.; Huang, W.L.; Lin, K.S. The assessment of reuse potential for municipal solid waste and refuse-derived fuel incineration ashes. *Resour. Conserv. Recycl.* **1999**, *25*, 255–270. [CrossRef]
16. Kong, L.; Xu, L.; Du, Y.; Jin, J.; Loprencipe, G.; Moretti, L. Use of Hybrid Mineral Filler with High Emissivity in Asphalt Mixture for Cooling Road Pavements. *Materials* **2022**, *16*, 175. [CrossRef]
17. Hoy, M.; Horpibulsuk, S.; Arulrajah, A. Strength development of Recycled Asphalt Pavement—Fly ash geopolymer as a road construction material. *Constr. Build. Mater.* **2016**, *117*, 209–219. [CrossRef]
18. Phummiphan, I.; Horpibulsuk, S.; Rachan, R.; Arulrajah, A.; Shen, S.-L.; Chindaprasirt, P. High calcium fly ash geopolymer stabilized lateritic soil and granulated blast furnace slag blends as a pavement base material. *J. Hazard. Mater.* **2018**, *341*, 257–267. [CrossRef] [PubMed]
19. Hoy, M.; Horpibulsuk, S.; Rachan, R.; Chinkulkijniwat, A.; Arulrajah, A. Recycled asphalt pavement-fly ash geopolymers as a sustainable pavement base material: Strength and toxic leaching investigations. *Sci. Total Environ.* **2016**, *573*, 19–26. [CrossRef]

20. Mohammed, B.S.; Adamu, M.; Liew, M.S. Evaluating the effect of crumb rubber and nano silica on the properties of high volume fly ash roller compacted concrete pavement using non-destructive techniques. *Case Stud. Constr. Mater.* **2018**, *8*, 380–391. [CrossRef]
21. Du, Y.; Ling, X.; Haibin, D.; Deyi, D.; Hao, W.; Weidong, L. Evaluation of thermal behavior and high-temperature performances of asphalt mixture containing fly ash cenosphere. *Constr. Build. Mater.* **2020**, *245*, 118429. [CrossRef]
22. Du, Y.; Xu, L.; Deng, H.; Deng, D.; Ma, C.; Liu, W. Characterization of thermal, high-temperature rheological and fatigue properties of asphalt mastic containing fly ash cenosphere. *Constr. Build. Mater.* **2020**, *233*, 117345. [CrossRef]
23. Di Mascio, P.; Loprencipe, G.; Moretti, L. Economic Evaluation of Cement Grouted Bituminous Mixes for Airport Pavements. *Materials* **2021**, *14*, 7230. [CrossRef]
24. Trunzo, G.; Moretti, L.; D'Andrea, A. Life Cycle Analysis of Road Construction and Use. *Sustainability* **2019**, *11*, 377. [CrossRef]
25. Moretti, L.; Cantisani, G.; Carpiceci, M.; D'Andrea, A.; Del Serrone, G.; Di Mascio, P.; Loprencipe, G. Effect of Sampietrini Pavers on Urban Heat Islands. *Int. J. Environ. Res. Public Health* **2021**, *18*, 13108. [CrossRef]
26. *JTG E20-2011*; Standard Test Methods of Bitumen and Bituminous Mixtures for Highway Engineering. Chinese Standard: Beijing, China, 2011.
27. *AASHTO TP-12*; Multiple Stress Creep Recovery (MSCR) Test of Asphalt Binder Using a Dynamic Shear Rheometer (DSR). AASHTO: Washington, DC, USA, 2012.
28. Kumar, R.; Saboo, N.; Kumar, P.; Chandra, S. Effect of warm mix additives on creep and recovery response of conventional and polymer modified asphalt binders. *Constr. Build. Mater.* **2017**, *138*, 352–362. [CrossRef]
29. *AASHTO TP 101-12*; Standard Method of Test for Estimating Fatigue Resistance of Asphalt Binders Using the Linear Amplitude Sweep. AASHTO: Washington, DC, USA, 2018.
30. Wang, C.; Zhang, H.; Castorena, C.; Zhang, J.; Kim, Y.R. Identifying fatigue failure in asphalt binder time sweep tests. *Constr. Build. Mater.* **2016**, *121*, 535–546. [CrossRef]
31. Witczak, M.W.; Kaloush, K.; Pellinen, T.; El-Basyouny, M.; Von Quintus, H. *Nchrp Report 465. Simple Performance Test for Superpave Mix Design*; Transportation Research Board: Washington, DC, USA, 2002.
32. Zhou, F.; Scullion, T.; Sun, L. Verification and Modeling of Three-Stage Permanent Deformation Behavior of Asphalt Mixes. *J. Transp. Eng.* **2004**, *130*, 486–494. [CrossRef]
33. *JTG F40-2004*; Technical Specifications for Construction of Highway Asphalt Pavements. Chinese Standard: Beijing, China, 2004.
34. Xu, L.; Zhao, Z.; Li, X.; Yuan, J.; Zhou, Q.; Xiao, F. Cracking investigation on fog seal technology with waterborne acrylate and polyurethane as a clean modification approach. *J. Clean. Prod.* **2021**, *329*, 129751. [CrossRef]
35. Cho, B.H.; Nam, B.H.; An, J.; Youn, H. Municipal Solid Waste Incineration (MSWI) Ashes as Construction Materials—A Review. *Materials* **2020**, *13*, 3143. [CrossRef]
36. Hassan, M.M.; Khalid, H.A. Compressive Deformation Behaviour of Asphalt Mixtures Containing Incinerator Bottom Ash Aggregate. *Road Mater. Pavement Des.* **2010**, *11*, 633–652. [CrossRef]
37. Chen, J.-S.; Chu, P.-Y.; Chang, J.-E.; Lu, H.-C.; Wu, Z.-H.; Lin, K.-Y. Engineering and Environmental Characterization of Municipal Solid Waste Bottom Ash as an Aggregate Substitute Utilized for Asphalt Concrete. *J. Mater. Civ. Eng.* **2008**, *20*, 432–439. [CrossRef]
38. Dongré, R.; D'Angelo, J.; Copeland, A. Refinement of Flow Number as Determined by Asphalt Mixture Performance Tester: Use in Routine Quality Control—Quality Assurance Practice. *Transp. Res. Rec. J. Transp. Res. Board* **2009**, *2127*, 127–136. [CrossRef]
39. Liu, H.; Luo, R.; Xi, L.; Hu, L. Development of Two-Step Secant Method to Interpret the Flow Number Test Data of Asphalt Mixtures. *J. Mater. Civ. Eng.* **2020**, *32*, 111. [CrossRef]
40. Wang, H.; Zhan, S.; Liu, G.; Xiang, J. The effects of asphalt migration on the flow number of asphalt mixture. *Constr. Build. Mater.* **2019**, *226*, 442–448. [CrossRef]

Disclaimer/Publisher's Note: The statements, opinions and data contained in all publications are solely those of the individual author(s) and contributor(s) and not of MDPI and/or the editor(s). MDPI and/or the editor(s) disclaim responsibility for any injury to people or property resulting from any ideas, methods, instructions or products referred to in the content.